Supporting Information

Mangione et al. 10.1073/pnas.1317488111

SI Methods

Patients. The study was carried out in accordance with the Declaration of Helsinki and was approved by the Royal Free Hospital Ethics Committee. All patients provided informed written consent.

Histology. Amyloid deposits were identified in fresh-frozen tissue sections by alkaline alcoholic Congo red staining with pathognomonic green birefringence in cross-polarized light (1), and fibril types were determined by standard immunohistochemical methods.

Isolation and Chemical Characterization of ex Vivo Amyloid Fibrils. Amyloid fibrils were isolated from spleen specimens by water extraction after repeated homogenization in 140 mM NaCl, 10 mM Tris, 10 mM EDTA, 0.1% (wt/vol) NaN_3, 1.5 mM PMSF, pH 8.0. Lyophilized fibrils (60 μg) were separated on SDS 15% PAGE carried out under reduced conditions. After staining with colloidal Coomassie Blue, excised bands underwent in situ proteolytic digestion (2) before analysis of the extracted peptide mixtures by MALDI-MS (ABI SCIEX 4800 MALDI TOF-TOF mass spectrometer) and by nano LC-MS/MS (Agilent Technologies CHIP MS Ion Trap XCT Ultra with capillary 1100 HPLC system and a chip cube) with raw data analysis by in-house Mascot database searching (Matrix Science). Unstained fibril samples from the SDS/PAGE were transferred to a PVDF membrane, and the same protein bands were analyzed by N-terminal sequencing (Applied Biosystems Procise HT49 Protein Sequencer).

DNA Sequencing. Genomic DNA was extracted from anticoagulated whole blood. Transthyretin (TTR) exons were amplified by PCR and sequenced.

Recombinant TTR Production. Recombinant wild-type, Ser52Pro variant TTR, and other amyloidogenic TTR variants (Val30Met, Leu55Pro, and Val122Ile) were expressed and purified as previously described (3). For Ser52Pro TTR, the Stratagene Quik-Change site-directed mutagenesis kit was used with the primer sequence GGAAAACCAGTGAGCCTGGAGAGCTGCATG containing the underlined codon for proline at position 52.

Thyroxine Displacement Assay. Binding by recombinant Ser52Pro variant TTR was tested by measuring the concentration of competing ligands, mds84 and Tafamidis, able to displace 50% of ^{125}I-thyroxine bound by TTR, as previously described (4).

Equilibrium Denaturation. TTR stability at 0.10 mg/mL was studied as a function of the guanidine thiocyanate (Gdn-SCN) concentration in 50 mM phosphate, 1 mM EDTA, 1 mM DTT, pH 7.0, at 25 °C for 24 h. Denaturation curves were derived from the ratio of tryptophan fluorescence emission intensities at 355 nm (unfolded) and 335 nm (folded) following excitation at 295 nm (Perkin-Elmer LS55 spectrofluorimeter) (5).

Microscopy Analyses. For electron and atomic force microscopy analyses, PMSF to 1 mM was added to Ser52Pro TTR fibrils, obtained as described in the main text, and the fibrils then were centrifuged at 10,600 × *g* and were resuspended twice before dilution 1:10 with water. After two washings, fibrils also were analyzed by SDS 15% PAGE under reducing conditions.

Electron Microscopy. Formvar-coated copper electron microscopy grids were placed coated-side down onto each sample and were incubated for 2 min before blotting with filter paper to remove excess solvent and staining with 2% (wt/vol) uranyl acetate for 2 min. After further blotting and drying in air, transmission electron microscope (CM120) images were obtained at 80 keV.

Atomic Force Microscopy. A 10-μL aliquot of fibrils was deposited on freshly cleaved mica and was dried under mild vacuum. Tapping mode atomic force microscopy images were acquired in air (Dimension 3000 SPM with "G" scanning head, maximum scan size 100 μm, driven at 320–340 kHz with scan rate 0.5–1.0 Hz by Digital Instruments, Veeco, Nanoscope IIIa controller and Olympus OMCL-AC160TS single-beam uncoated silicon cantilevers).

X-Ray Fiber Diffraction. Ser52Pro TTR fibrils were diluted to ∼10 mg/mL in filtered MilliQ water and were allowed to align between two wax-tipped capillary tubes. The partially aligned sample was mounted on a goniometer head, and X-ray diffraction data were obtained with a Rigaku CuKα (λ 1.5419 Å) rotating anode generator and were collected using VariMax-HF mirrors and a Saturn 944+ CCD detector with exposure times of 15–30 s and a specimen-to-detector distance of 50 or 100 mm. Diffraction data were displayed using Mosflm and converted to a TIFF file for inspection in Clearer (6).

X-Ray Crystal Structure Determination. Orthorhombic protein crystals were grown by hanging-drop vapor diffusion at pH 7.4 using PEG400 as the precipitant (7). X-ray diffraction data were collected on beamline I04 and I04-1 at the Diamond Light Source, Oxfordshire, United Kingdom; diffraction images were integrated by XDS (8) scaled by SCALA (9), and phases were determined by molecular replacement with PHASER (10) using PDB code 1DVQ as the search model. Protein models were built with COOT (11) and refined with REFMAC (12).

Cross-Seeding Fibrillogenesis. Thioflavin T (ThT) emission in the 96-well black-wall plate containing wild-type and Ser52Pro TTR was monitored in the presence of 0.1 mg/mL Ser52Pro TTR fibrils produced with trypsin and then treated with PMSF. Relative intensities of fluorescence were monitored in three replicate test and control wells for the next 7 h.

Mass Spectrometry Analysis of Native TTR–Retinol-Binding Protein Complex. Isolated retinol-binding protein (RBP) (Sigma) was incubated with one molar equivalent of retinol to produce holo-RBP. Both the holo-RBP and isolated recombinant Ser52Pro TTR were buffer exchanged into 200 mM ammonium acetate (pH 7.4) using Micro Bio-Spin size-exclusion chromatography columns (BioRad). Protein concentrations were determined by A_{280} 26,595 and 18,450 $M^{-1}\cdot cm^{-1}$ for RBP and TTR, respectively. Mixtures of TTR with two molar equivalents of holo-RBP were loaded into in-house–prepared glass capillaries for nano-electrospray analysis (13) using a Q-TOFII instrument (Micromass) modified for the transmission of large complexes (14). Capillary, cone, and transfer voltages were 1.7 kV, 100 V, and 10 V, respectively, with the backing pressure in the transfer region at 8.8 mbar. Calibration was with cesium iodide at 100 mg/mL, and mass spectra were analyzed with MassLynx V4.1.

Amyloid Fibrillogenesis with Natural Ligands. Amyloid fibrillogenesis was carried out in the presence of a twofold molar excess of either thyroxine or holo-RBP. Pre- and posttrypsin (4 h) digestion samples were analyzed by SDS 15% PAGE under reducing conditions as described above.

1. Putchler H, Sweat F, Levine M (1962) Binding of Congo Red by amyloid. *J Histochem Cytochem* 10:355–364.
2. Troise F, et al. (2011) A novel ErbB2 epitope targeted by human antitumor immunoagents. *FEBS J* 278(7):1156–1166.
3. Lashuel HA, Lai Z, Kelly JW (1998) Characterization of the transthyretin acid denaturation pathways by analytical ultracentrifugation: Implications for wild-type, V30M, and L55P amyloid fibril formation. *Biochemistry* 37(51):17851–17864.
4. Kolstoe SE, et al. (2010) Trapping of palindromic ligands within native transthyretin prevents amyloid formation. *Proc Natl Acad Sci USA* 107(47):20483–20488.
5. Hammarström P, Wiseman RL, Powers ET, Kelly JW (2003) Prevention of transthyretin amyloid disease by changing protein misfolding energetics. *Science* 299(5607):713–716.
6. Makin OS, Sikorski P, Serpell LC (2007) CLEARER: A new tool for the analysis of X-ray fibre diffraction patterns and diffraction simulation from atomic structural models. *Appl Cryst* 40(5):966–972.
7. Trivella DB, Sairre MI, Foguel D, Lima LM, Polikarpov I (2011) The binding of synthetic triiodo l-thyronine analogs to human transthyretin: Molecular basis of cooperative and non-cooperative ligand recognition. *J Struct Biol* 173(2):323–332.
8. Kabsch W (2010) XDS. *Acta Crystallogr D Biol Crystallogr* 66(Pt 2):125–132.
9. Evans P (2006) Scaling and assessment of data quality. *Acta Crystallogr D Biol Crystallogr* 62(Pt 1):72–82.
10. McCoy AJ, et al. (2007) Phaser crystallographic software. *J Appl Cryst* 40(Pt 4):658–674.
11. Emsley P, Cowtan K (2004) Coot: Model-building tools for molecular graphics. *Acta Crystallogr D Biol Crystallogr* 60(Pt 12 Pt 1):2126–2132.
12. Murshudov GN, et al. (2011) REFMAC5 for the refinement of macromolecular crystal structures. *Acta Crystallogr D Biol Crystallogr* 67(Pt 4):355–367.
13. Hernández H, Robinson CV (2007) Determining the stoichiometry and interactions of macromolecular assemblies from mass spectrometry. *Nat Protoc* 2(3):715–726.
14. Sobott F, Hernández H, McCammon MG, Tito MA, Robinson CV (2002) A tandem mass spectrometer for improved transmission and analysis of large macromolecular assemblies. *Anal Chem* 74(6):1402–1407.

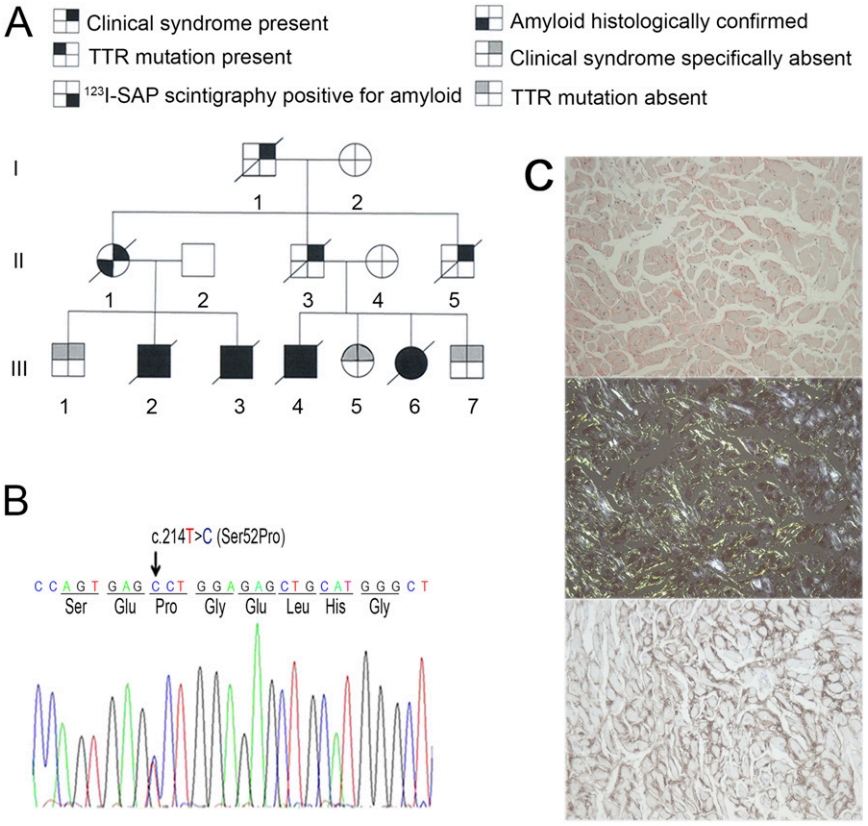

Fig. S1. Hereditary Ser52Pro TTR amyloidosis. (*A*) Pedigree of the affected kindred. Squares indicate males; circles indicate females; slashes indicate deceased kindred. (*B*) Partial sequence chromatogram of exon 4 of the TTR gene showing the nucleotide substitution identified in affected family members. (*C*) Abundant cardiac amyloid in patient. (*Top*) Congo red stain, bright field. (*Middle*) Congo red stain, cross-polarized light. (*Bottom*) Immunohistochemical stain with anti-TTR antibody.

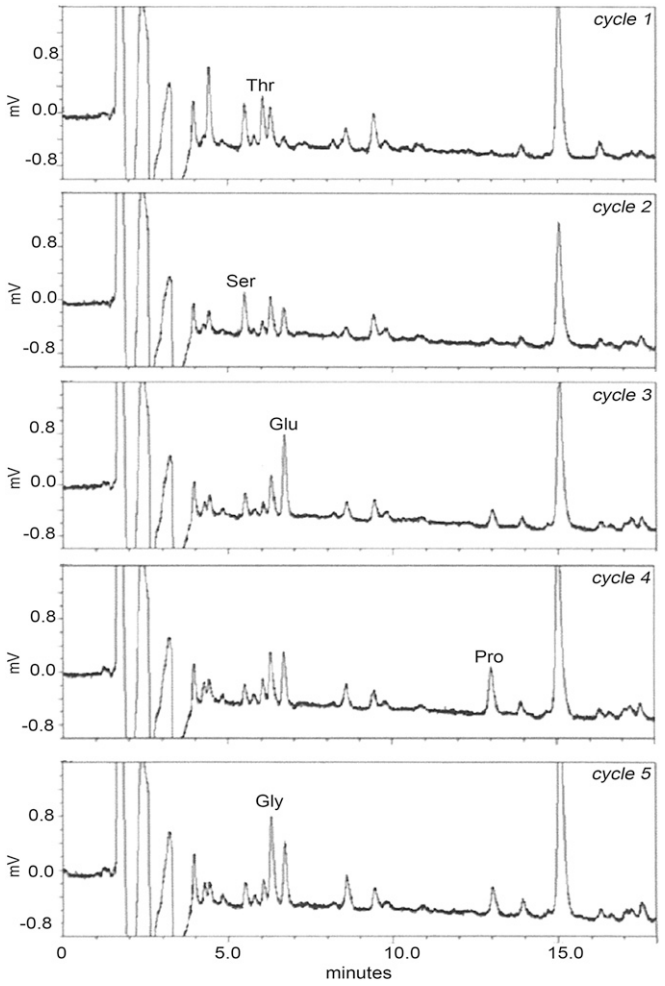

Fig. S2. N-terminal sequence of TTR fragment from ex vivo amyloid fibrils. Five cycles of Edman N-terminal sequencing of band 2 from the SDS/PAGE in Fig. 1*B*, which had been blotted onto PVDF membrane, yielded the sequence Thr-Ser-Glu-Pro-Gly, corresponding to residues 49–53 of variant TTR with Pro in position 52.

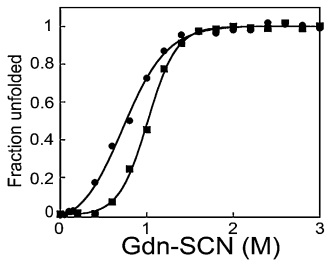

Fig. S3. Thermodynamic stability of wild-type and Ser52Pro TTR. Gdn-SCN denaturation curves of wild-type TTR (squares) and Ser52Pro variant TTR (circles). Experimental data were fitted to a single transition as described (1) and were converted to the unfolded fraction using $f_U = (y - y_N)/(y_U - y_N)$, where y is the ratio between 355 nm and 335 nm fluorescence emission intensities at a given denaturant concentration and y_N and y_U are the values of native and unfolded protein, respectively, extrapolated from the pre- and posttransition baselines.

1. Hammarström P, Wiseman RL, Powers ET, Kelly JW (2003) Prevention of transthyretin amyloid disease by changing protein misfolding energetics. *Science* 299(5607):713–716.

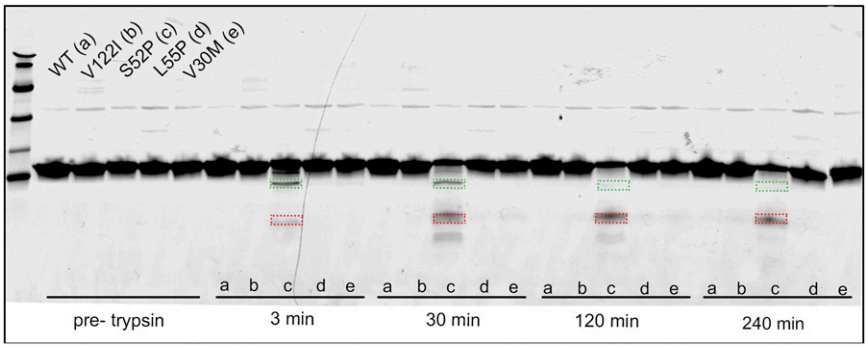

Fig. S4. Limited in vitro tryptic proteolysis cleaves Ser52Pro but not other TTR isoforms. SDS 15% PAGE under reducing conditions of wild-type (a), Val122Ile (b), Ser52Pro (c), Leu55Pro (d), and Val30Met TTR (e) after incubation at 37 °C with trypsin at an enzyme:substrate ratio of 1:200 for the times shown. The peptides 49-127 and 81-127 released from Ser52Pro TTR are highlighted in green and red boxes, respectively.

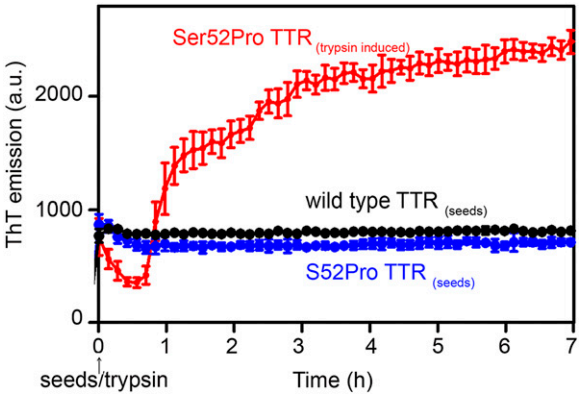

Fig. S5. Cross-seeding fibrillogenesis experiments. Relative intensities of ThT emission, after subtraction of the pretrypsin fluorescence, were plotted. Means (SD) of three replicates are shown.

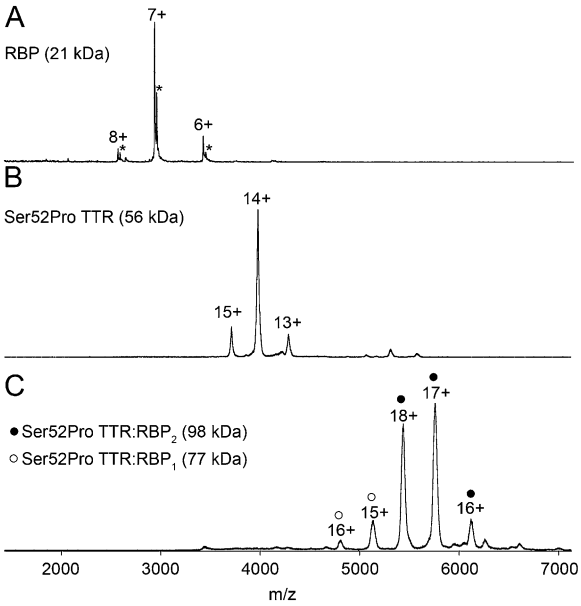

Fig. S6. Mass spectrometry of the native Ser52Pro TTR–RBP_2 complex. Mass spectra were obtained for (*A*) monomeric RPB; asterisks indicate the presence of retinol bound by RBP, (*B*) tetrameric Ser52Pro TTR, and (*C*) Ser52Pro TTR–RBP_2 complex.

Table S1. Binding of stabilizers by TTR

	Mean IC_{50}, μM (SD)	
Ligand	Wild-type TTR	Ser52Pro TTR
mds84	0.13 (0.02)	0.14 (0.02)
Tafamidis	0.3 (0.04)	0.3 (0.05)

Comparative binding capacity of wild-type and Ser52Pro variant TTR measured by displacement of the natural ligand, thyroxine, in the presence of increasing concentrations of two potent stabilizers (1). IC_{50} values represent the ligand concentration reducing the binding of ^{125}I-thyroxine by wild-type and Ser52Pro variant TTR by 50%. $n = 3$.

1. Kolstoe SE, et al. (2010) Trapping of palindromic ligands within native transthyretin prevents amyloid formation. *Proc Natl Acad Sci USA* 107(47):20483–20488.

Table S2. Thermodynamic parameters of Gdn-SCN–induced unfolding

	C_m,	$\Delta G°(H_2O)$, kcal·mol^{-1}	m, kcal·mol^{-1}·M^{-1}
Wild-type TTR	1.03 (0.02)	4.42 (0.25)	4.31 (0.32)
Ser52Pro TTR	0.80 (0.06)	2.11 (0.50)	2.58 (0.44)

The change of fluorescence as a function of denaturant concentration was analyzed as previously reported (1). Values of midpoint denaturant concentration (C_m), free energy in the absence of denaturant [$\Delta G°(H_2O)$], and dependence of ΔG on denaturant concentration (m value) are shown as mean (SD) of three independent experiments.

1. Santoro MM, Bolen DW (1988) Unfolding free energy changes determined by the linear extrapolation method. 1. Unfolding of phenylmethanesulfonyl α-chymotrypsin using different denaturants. *Biochemistry* 27(21):8063–8068.

Table S3. Crystallographic statistics

Structure	Wild-type TTR	Ser52Pro TTR
PDB code	4MRB	4MRC
Beamline	DLS I04-1	DLS I04
Wavelength, Å	0.920	0.979
Space group	$P2_12_12$	$P2_12_12$
Cell dimensions, Å	84.21 × 41.32 × 63.01	85.41 × 42.02 × 63.68
Resolution, Å	42.10–1.27	85.41–1.54
Completeness, %	99.7	99.7
Multiplicity	12.9	4.9
Total reflections	754.151	170.272
Unique reflections	58.650	34.619
R_{merge}/R_{pim} (±)*	0.057 (0.626)/0.024 (0.266)	0.055 (0.573)/0.019 (0.433)
Reflections used for R-free value	2,962	1,742
RMSD of bond length(Å)/angles, degrees	0.033/2.79	0.019/1.78
R/R-free value	0.166/0.209	0.160/0.228

*Values in parenthesis are for the highest-resolution shell.